Collective Transport for Nonlinear Current-Voltage Characteristics of Doped Conducting Polymers

Jiawei Wang,[1,2] Dongyang Liu,[1,2] Lishuai Yu,[3] Feilong Liu,[3] Jiebin Niu,[1] Guanhua Yang,[1] Congyan Lu,[1] Nianduan Lu,[1] Ling Li,[1,2,*] and Ming Liu[1,2]

[1]*Key Laboratory of Microelectronic Devices and Integrated Technology, Institute of Microelectronics of Chinese Academy of Sciences, Beijing 100029, China*

[2]*University of Chinese Academy of Sciences, Beijing 100049, China*

[3]*South China Academy of Advanced Optoelectronics, South China Normal University, Guangzhou 510006, People's Republic of China*

(Received 15 December 2021; revised 26 September 2022; accepted 3 April 2023; published 26 April 2023)

Origin of nonlinear transport phenomena in conducting polymers has long been a topic of intense controversies. Most previous knowledge has attributed the macroscopic nonlinear *I-V* characteristics to individual behaviors of elementary resistors in the network. In this Letter, we show via a systematic dimensionality-dependent transport investigation, that understanding the nonlinear transport in conducting polymers must include the collective transport effect in a percolation network. The possible mediation of percolation threshold p_c by controlling the samples' dimensionality unveiled the collective effect in growth of percolation paths driven by electric field, enabling us to draw a smooth connection between two typically observed nonlinear phenomena, dissipative tunnelinglike and threshold-limited transport, which have been controversial for years. The possible microscopic origins of the collective transport are discussed within the Coulomb blockade theory.

DOI: 10.1103/PhysRevLett.130.177001

Charge transport in conducting polymers has been intensively investigated over the past years since these polymers not only demonstrate great application potential in future electronics but also represent a prototype of electronic disordered systems with a strong localization effect [1–3]. The macroscopic conduction of such systems has always been simplified as elementary hopping depicted with statistical parameters such as the average hopping distance or effective energetic disorder [3–5], and such homogeneous treatment has demonstrated success in modeling most of the electrical behaviors in disordered polymeric systems. Typically, in the longstanding controversial topic of the origin of nonlinear transport behaviors in conducting polymers [6–13], the non-Ohmic current-voltage (*I-V*) characteristics have been widely simplified into the tunnelings at elementary resistors in the network [6,8–11]. In detail, the universal scaling behaviors have been reified into the individual nonlinear excitations in Luttinger liquids [6], nuclear tunneling [8], or other hopping junctions described by the dissipative tunneling (DT) formula [14,15].

While there have also been studies claiming a threshold-limited (TL) nonlinear *I-V* phenomenon, especially in mesoscopic devices based on polymers [7,13], the totally insulating behavior below a critical voltage threshold suggests the possible existence of collective transport in conducting polymers and thus reveals the deficiencies of homogeneous approaches.

Interestingly, in this Letter, we realize simultaneous observations of both typically reported nonlinear phenomena (DT-like and TL-like) by simply varying the polymer films' thickness from 2D single molecular layer to 3D multilayer. We propose that a framework emphasizing the collective transport in inhomogeneous media could naturally unify the phenomena, based on the possible mediation effects from the dimensionality on percolation threshold p_c. That the sequential growth of percolation paths in collective transport greatly contributes to macroscopic nonlinear transport behavior in conducting polymers is central.

We investigated the doped polymeric material poly[2,5-bis(3-dodecylthiophen-2-yl)thieno[3,2-b]thiophene] (C14-PBTTT), which exhibits an ideal layer-by-layer stacking character, and two other materials, poly(3-hexylthiophene-2,5-diyl) (P3HT) and poly(4,4''-didodecyl[2,2:5,2:5,2-quaterthiophene]-5,5-diyl) (C12-PQT). The polymers with the "edge-on" molecular stacking character show a layer-by-layer growth mode at the molecular scale, and the second molecular layer begins to form at the completion of the first layer. This property enables us to realize control of the film thickness at the molecular level. By controlling the solution casting conditions, including the polymer solution concentration [16], we precisely layered polymer films with thicknesses from the 2D subsingle molecular layer to the bilayer and more than tens of nanometers, denoted as 3D samples. Atomic force microscopy (AFM) was used to characterize the 2D quasi-single molecular layer and 3D thick film containing multiple monolayers of PBTTT, as shown in Fig. 1(a). The thickness-controllable growth of P3HT and PQT was characterized by AFM, as shown in the

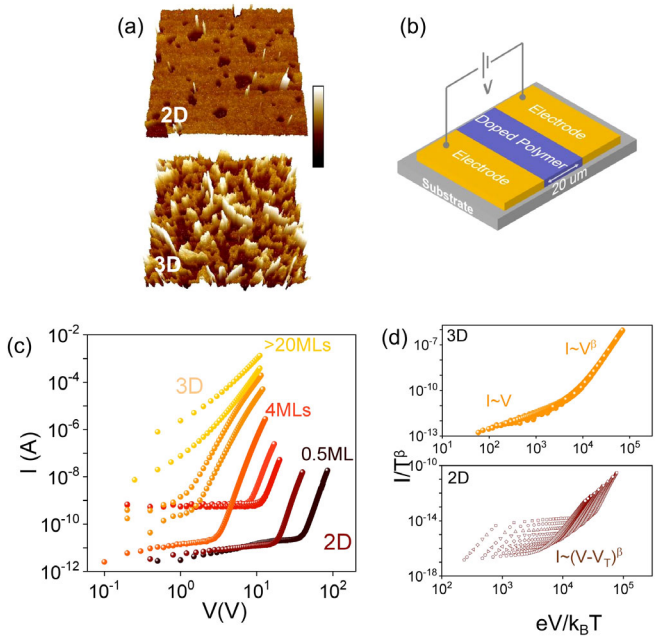

FIG. 1. (a) AFM images of precisely layered polymer films (PBTTT-C14) of 2D (single or subsingle molecular layer) and multilayer (approximately 50 nm thick) denoted as 3D. (b) Schematic of the device structure. (c) Dimensionality or film thickness-dependent nonlinear I-V curves at $T = 6$ K for PBTTT-C14-based devices, in logarithmic coordinates. (d) Scaled I-V curves for the 3D sample at temperatures ranging from 6 to 50 K, universally depicted via the DT model by plotting I/T^{β} versus eV/k_BT; for the 2D samples, blocked behavior led to failure in scaling with the DT model.

Supplemental Material [16]. The films were doped with 2,3,5,6-tetrafluoro-7,7,8,8-tetracyanoquinodimethane (F_4TCNQ) via a solid-state diffusion approach [17], and the doping level was approximately 15%, corresponding to a hole concentration of approximately 1×10^{20} cm^{-3}. Transport properties (I-V curves) were measured with the two-terminal devices with channel length $L = 20$ μm schematically shown in Fig. 1(b). Graphene was patterned as the bottom electrode, and the selection of graphene as the contact was due to the ultrathin nature, which could maintain the continuity and morphology of the monolayer polymer. The influence of the contact resistance was negligible, as analyzed by 4 probe devices [16].

The dimensionality-dependent nonlinear transport at low temperature was characterized with the device structure displayed in Fig. 1(b). Interestingly, as shown in Fig. 1(c), the nonlinear I-V curves (data from PBTTT-based devices) displayed in logarithmic coordinates exhibit distinct behaviors for the two extreme cases of two and three dimensions. The curves for the 3D multilayer samples feature Ohmic behavior ($I \sim V$) at lower fields ($eV \ll k_BT$) and power-law-type nonlinear behavior ($I \sim V^{\beta}$) at higher fields ($eV \gg k_BT$). More remarkably, the I-V curves in a specific temperature range could be universally scaled down onto a single curve, as depicted by DT theory, shown in Fig. 1(d). These coincide with the widely reported universal phenomena [6,8,11], in which the nonlinear I-V curves were generally attributed to the nonlinearity at elementary junctions of Luttinger liquids, nuclear tunneling, or others. However, such behavior did not hold when the polymer films were thinned to the 2D limit, as shown in Fig. 1(c). More specifically, none of the I-V curves for 2D films feature an Ohmic character at lower fields ($eV \ll k_BT$); instead, they exhibit threshold-limited behaviors with unidentified currents and directly enter the nonlinear region with the onset of conduction at a higher bias [16]. The behavior is well described by the relation

$$I = I_0(V - V_T)^{\beta}, \tag{1}$$

derived for depicting the collective charge transport in gold dot arrays [18–20], with the current intensity being proportional to the quantity of percolation paths. I_0 is the prefactor, and V_T is defined as the threshold voltage related to the minimal value for biasing the sample so that it is conductive. Similar behaviors attributed to Coulomb blockade have also been frequently reported in polymer- and other material-based mesoscopic devices [7,13,20].

While the dimensionality effect enables a possible correlation between the two typically observed types of nonlinear transport (DT-like and TL-like), we show that such a unified connection can be naturally realized by including the collective transport in inhomogeneous media. In the low-temperature case, as in our experiments, transport in disordered materials should be dominated by field-driven tunneling between ground states, as shown in Fig. 2(a). With the suppression of the phonon activation strength, tunneling occurs only when the voltage drop across the junction equals the barrier potential height $eV_r = E_b$. The tunneling process can be quantitatively described via deduction of Fermi's golden rule,

$$k = A\left[-\frac{E_b - eV_r}{1 - \exp[(E_b - eV_r)/k_BT]} + \frac{E_b + eV_r}{1 - \exp[(E_b + eV_r)/k_BT]}\right], \tag{2}$$

where k is the tunneling rate and A is a prefactor related to the carrier delocalization degree and tunneling distance. Curves of the k-V_r relation with different tunneling barriers at $T = 6$ K are displayed in Fig. 2(b), exhibiting clear threshold-limited behavior. When k_BT overcomes the barrier, the tunneling shows an Ohmic I-V relation, while when E_b far exceeds the strength of k_BT, conduction only occurs in the regime $eV_r \geq E_b$.

The distribution of the elementary barrier height E_b along possible paths of the network is assumed to represent the energetic inhomogeneity of the media, as shown in Fig. 2(c). In the zero-bias limit, the finite thermal strength

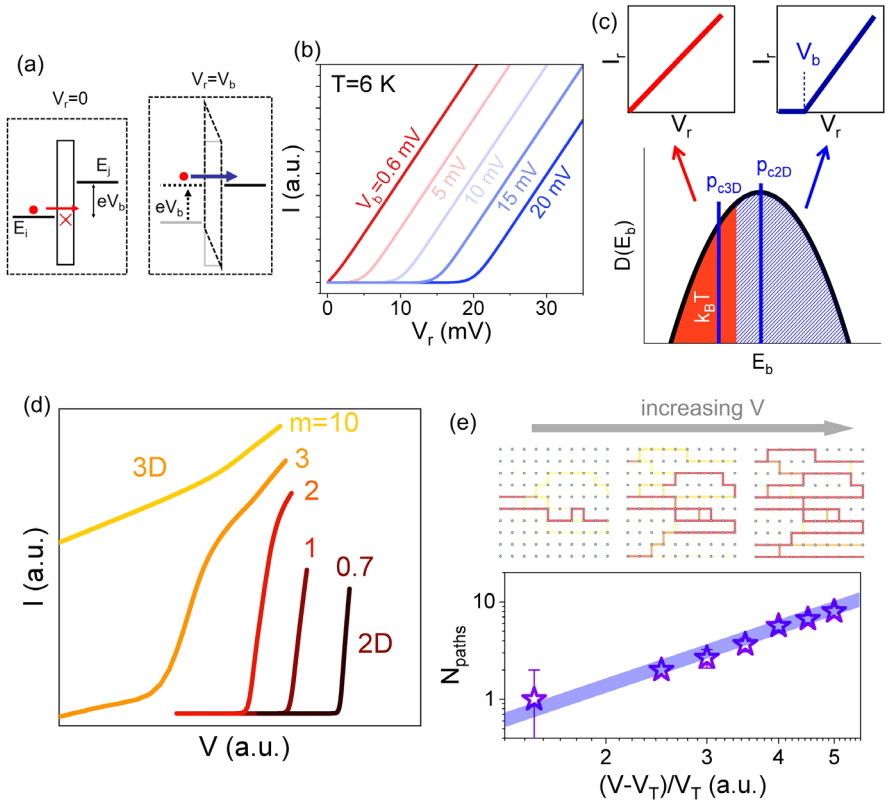

FIG. 2. (a) Schematic of the tunneling process between ground states. (b) I-V curves of the tunneling process at resistors of different barrier heights at $T = 6$ K. (c) Distribution of elementary barrier heights E_b, composed of a conducting ($k_BT > E_b$) portion (red) and an insulating or blocked portion ($k_BT < E_b$); the inset shows the I_r-V_r curve of individual resistors in the conducting (left) and insulating (right) portions of the network. (d) Simulated nonlinear transport behavior from 2D to 3D inhomogeneous networks. (e) Percolation paths' growth driven by electric bias.

(k_BT) makes a portion (p) of resistors with smaller barriers ($E_b < k_BT$, red region) conduct, while the other portion (1-p) ($E_b > k_BT$) of resistors behave in an insulating manner. For macroscopic conduction of the whole network, the relative location of p_c in the distribution is the key point. Under the premise of the distinct I-V curves in the 2D and 3D cases and considering the dependence of p_c on the dimensionality [21,22], we anticipate that generally, the portion p is higher than the 3D threshold p_{c3d} but lower than p_{c2d}. Consequently, we divided the I-V curves for cases from 2D to 3D into three regimes: (i) the *Ohmic regime* in 3D samples, where percolation paths form with Ohmic conduction due to $p > p_{c3d}$; (ii) the *blocked regime* in 2D samples, where no conducting path exists due to $p < p_{c2d}$; and (iii) the *nonlinear regime* in both samples, where electric bias V-induced breakthrough of the insulating portion in the network leads to collective transport based on the growth of new percolation paths $n \sim (V - V_T)^{\gamma}$.

Remarkably, we reconstructed experimental dimensionality-dependent nonlinear transport by simulating the layer thickness-mediated collective percolation in inhomogeneous resistor networks. We employed $10 * m * 10$ networks for simulating both the 2D and 3D cases ($m \leq 1$ for the 2D case). The inhomogeneity was introduced with random fluctuations of the barrier height depicted by a lognormal function [16], in addition to randomly located vacancies in the networks. The tunneling rate obtained by Eq. (2) was employed to depict the barrier-limited charge transfer between ground states at each resistor. The simulated network I-V curves are displayed in Fig. 2(d). The 2D cases exhibit larger blocked regions (could also be quantified with V_T) and exponents β; with thickening of the films to 3D cases, the blocked region shrinks and finally disappears with the onset of the Ohmic region, and the exponent β decreases. All these results ideally mimic the experimentally obtained nonlinear curves and their dimensionality dependence. The simulated percolation paths in the resistor network at various biases are displayed in Fig. 2(e) and the Supplemental Material [16], the quantity of onset paths is well plotted in a power-law relation with the bias $n \sim (V - V_T)^{\gamma}$ [18,20], indicating the collective transport nature.

For deeper insights into the origin of the collective transport, the structural information of polymer films (PBTTT, 8 nm thick film) was investigated by dark field-transmission electron microscopy (DF-TEM). As shown in Fig. 3(a), by locking only a specific part of the (010) ring in the selected area electron diffraction

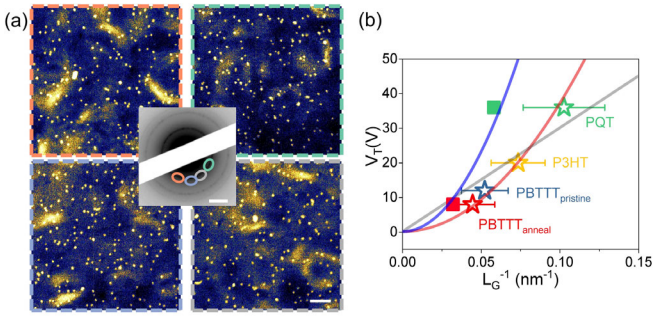

FIG. 3. (a) DF-TEM images of a traditional semicrystalline conjugated polymer (PBTTT-C14) film, by locking specifically oriented (010) rings in SAED in the middle inset. The scale bar is 200 nm for DF-TEM and 2 nm^{-1} for SAED. (b) Relation between V_T and L_G^{-1} in different polymeric samples; red and gray lines are the parabolic and linear fittings, respectively.

(SAED, shown inset), as marked by the circles, crystalline segments, including 2D flakelike grains and larger domains of specific orientations, were evidently visualized as brighter regions in the DF-TEM images. In the figures related to crystallinity imaged under four different incidence directions of the tilted electron beam, the micro-orientation is totally random. The grain sizes inhomogeneously range from 15 to more than 40 nm, and the most dominant grains for pristine and annealed PBTTT films are $L_G = 25$ and 20 nm, respectively, while for P3HT and PQT, the sizes are approximately 15 and 10 nm, respectively, almost at the resolution limit [16].

Assuming that tunneling occurs between ordered regions such as the grains or domains, V_T should be related to the numbers of barriers overcome, $V_T \sim N \sim 1/L_G$. We experimentally found that the V_T values from 2D devices based on the three materials are approximately in a parabolic relation with the reciprocal of the grain size $V_T \sim (1/L_G)^2$, as shown in Fig. 3(b), indicating that transport is not limited only by the number of tunneling junctions. The underlying relation suggests a possible compatibility with Coulomb charging-related tunneling processes, in which the tunneling barrier is related to the charging energy and inversely proportional to the island size, $E_c \sim e^2/C \sim e^2/L_G$, finally leading to $V_T \sim NE_c \sim (1/L_G)^2$.

To be more quantitative in how the conducting (p) and insulating (1-p) portions correlate with the samples' dimensionality in an assumed Coulomb charging limited transport network, the layer thickness-dependent V_T values were investigated by considering the underlying relation between layer thickness L_{th} and p_c. As shown in Fig. 4(a), we extracted the V_T in samples of various L_{th}s for PBTTT samples [16]. At the crossover from 2D ($L_{\mathrm{th}} \leq 1$ ML) to thicker film cases, V_T gradually decreases from above 10 to 0 V.

As shown in Fig. 4(b), the values of p_c at different film thicknesses ranging from 2D to 3D were determined by [22]

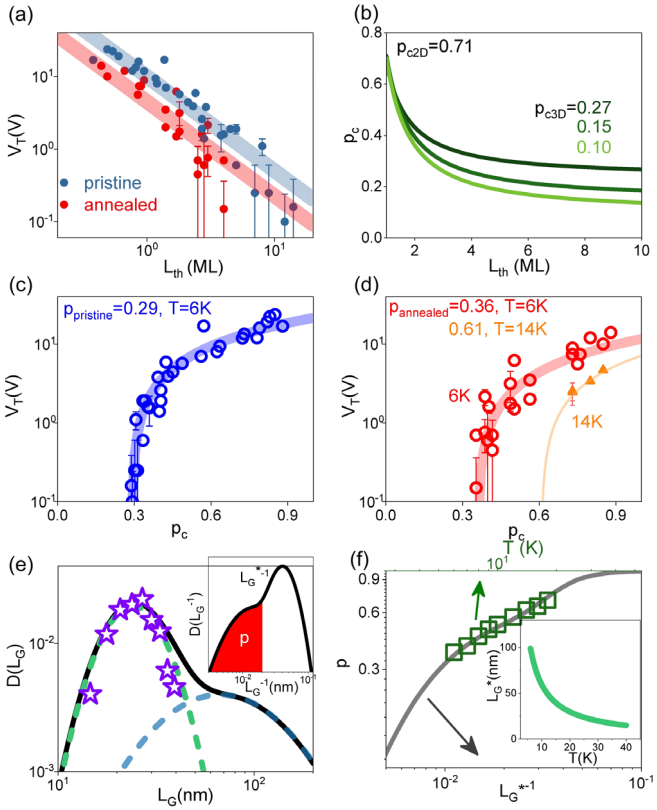

FIG. 4. (a) Extracted threshold voltage V_T in PBTTT-C14 samples and its dependence on the film thicknessor dimensionality. (b) Layer thickness dependence of percolation threshold p_c, with $p_{c2D} = 0.71$ and $p_{c3D} = 0.27$, 0.15, and 0.1. (c) and (d) Relations between V_T and p_c for pristine PBTTT films (c) at $T = 6$ K and for annealed PBTTT (d) at $T = 6$ and 14 K, assuming $p_{c\infty} = 0.27$. The data were well fitted by $V_T = A(p_c - p)$. (e) Dual lognormal distribution of the segment sizes (L_G) in PBTTT polymer films, including the crystalline grain (green dashed) and domain (blue dashed) sizes. The inset shows the distribution of the reciprocal of L_G. (f) p-L_G^{*-1} relation corresponding to the p-T relation based on the function between L_G^* and T shown in the inset.

$$p_c(L_{\mathrm{th}}) \sim p_{c\infty} + \alpha \cdot L_{\mathrm{th}}^{-1/\nu}, \tag{3}$$

where $p_c(L_{\mathrm{th}})$ is the thickness-dependent percolation threshold, $p_{c\infty}$ is the percolation threshold as the layer thickness approaches infinity, L_{th} is in units of a single molecular layer thickness (approximately 2 nm for PBTTT), and v is the critical exponent (always, $v \approx 0.8$). We set $p_{c2D} = 0.71$, referring to the "site" percolation in the 2D Voronoi network approximation, which has always been employed to model semicrystalline systems [23,24], and $p_{c\infty} = 0.27$, 0.15, and 0.10 are chosen for the other boundary condition in Eq. (2) according to the results in 3D packed binary grain systems [25,26].

The values of $V_T(L_{\mathrm{th}})$ were plotted as a function of $p_c(L_{\mathrm{th}})$ by Eq. (3), as shown in Figs. 4(c) and 4(d). Assuming that conducting portion p is simply influenced

by temperature, the experimentally obtained V_T values well scale with the difference between percolation threshold p_c and conducting portion p

$$V_T(L_{\mathrm{th}}) = A(p_c(L_{\mathrm{th}}) - p(T))^{\chi}, \tag{4}$$

where A is a prefactor with units of voltage and χ is a dimensionless parameter that varies from approximately 0.8 to 1.3. We fixed $\chi = 1$ in different samples and at various temperatures for universality. This result corresponds with what has been predicted in the collective transport in nanometer-gold arrays [20]. As shown in Fig. 4(c), in the pristine PBTTT-based samples for $p_{c\infty} = 0.27$, we obtained conducting portion $p_{\mathrm{pristine}} = 0.295$ at $T = 6$ K, while the value increased to $p_{\mathrm{annealed}} = 0.36$ in the annealed samples shown in Fig. 4(d). A higher temperature leads to activation of a higher conducting portion and a lower V_T, and the fitting gives the value $p_{\mathrm{annealed}} = 0.61$ when the temperature is increased to $T = 14$ K. For the cases of P3HT and PQT and the situations of $p_{c\infty} = 0.15$ and 0.10, the results are displayed in the Supplemental Material [16].

The extracted $p(T)$ could be well correlated to the materials' structural data. A dual-lognormal distribution function $D(L_G)$ was employed to depict the size information of both grains (green dashed) and domains (blue dashed) in PBTTT, as shown in Fig. 4(e). Considering that larger segments are more easily charged, integration of the distribution function $D(L_G^{-1})$ [inset of Fig. 4(e)] enables us to obtain a p-L_G^{*-1} relation, as shown by the gray curve in Fig. 4(f), where L_G^* is the island size whose charging energy is just exactly overcome by the temperature, $2k_BT \sim e^2/(2C) = e^2/(8\varepsilon_r\varepsilon_0 L_G^*)$ [7,16]. We plotted p-L_G^{*-1} together with the p-T data (green symbols) obtained experimentally based on the underlying relation between T and L_G^* through the charging process shown in the inset of Fig. 4(f). We found that when setting an appropriate distribution for the domain sizes and using a relative dielectric constant $\varepsilon_r = 40$, the p-L_G^{*-1} curve could well correspond with the p-T relation in the PBTTT sample. The distribution of domain sizes employed for fitting has an extreme value of approximately $L_G = 70 - 80$ nm [blue dashed line in Fig. 4(e)], which is reasonable compared to the data from DF-TEM. $\mathcal{E}_r$'s value is in a reasonable range (10–100) for conducting polymers; actually, the value should be smaller when taking into account the coupling among the Coulomb islands, but such analysis could hardly be further quantitative due to the complexity of the polymer structure.

The existence of Coulombic charging-limited transport was further explored. Possible Coulomb oscillations were observed in several sub-100 nm devices, the channels of which contain only countable grains, whose charging process could be manifested in the steplike conductance of the I-V curves [16]. Additionally, the collective transport at the onset of nonlinearity features much larger conductivity fluctuations than that in the Ohmic region. This phenomenon could be well explained by the CB scenario [16].

However, CB is not a unique solution for the microscopic origin of the collective nonlinear transport in conducting polymers. On one hand, the quantitative analysis of the CB percolative network includes approximations and assumptions. Determining the L_{th}-dependent p_c is actually difficult due to the existence of the large degrees of anisotropy and disorder in the system when treating the grains as 2D metallic sheets; and p might vary with changing layer thickness, there are reports about the crystallinity change at increasing film thicknesses in organic semiconductors. However, these factors do not qualitatively affect our conclusions about the collective transport within the inhomogeneous network. On the other hand, due to the weak van der Waals interactions in molecular solids, various charge transfer mechanisms could coexist.

The dimensionality-related transport behavior enables us to gain new insights into the controversial topic of the nonlinear character in the I-V curves of polymers. Through modulation of the percolation threshold p_c, we find that the nonlinear transport cannot be simplified into the elementary behavior of a tunneling junction or a hopping unit in the network but arises from the collective behavior of charge carriers percolating along various paths. The great inhomogeneity in the polymer microstructure leads to nonuniform onset of conduction for different percolation paths. Monte Carlo simulation could well reconstruct the dimensionality dependent nonlinear transport with considering the collective transport effect. The possible correlations between CB effect and the insulating resistors in the network are discussed, which shows that the CB effect is compatible with both the electrical behavior and the structural inhomogeneity.

This work was supported by the National Key R&D Program of China (Grant No. 2018YFA0208503), by the Opening Project of Key Laboratory of Microelectronic Devices and Integrated Technology, Institute of Microelectronics, Chinese Academy of Sciences, and by the National Natural Science Foundation of China (Grants No. 61890944, No. 92264204, No. 62274178, No. 61720106013, No. 61904195, and No. 62004214), by the Strategic Priority Research Program of Chinese Academy of Sciences (Grants No. XDB30030000, and No. XDB30030300).

*Corresponding author.
lingli@ime.ac.cn

[1] Rodrigo Noriega, Jonathan Rivnay, Koen Vandewal, Felix P. V. Koch, Natalie Stingelin, Paul Smith, Michael F. Toney, and Alberto Salleo, Nat. Mater. **12**, 1038 (2013).
[2] R. S. Kohlman, A. Zibold, D. B. Tanner, G. G. Ihas, T. Ishiguro, Y. G. Min, A. G. MacDiarmid, and A. J. Epstein, Phys. Rev. Lett. **78**, 3915 (1997).

[3] Shawn A. Gregory, Riley Hanus, Amalie Atassi, Joshua M. Rinehart, Jamie P. Wooding, Akanksha K. Menon, Mark D. Losego, G. Jeffery Snyder, and Shannon K. Yee, Nat. Mater. **20**, 1414 (2021).
[4] V. Coropceanu, J. Cornil, D. A. da Silva Filho, Y. Olivier, R. Silbey, and J.-L. Brédas, Chem. Rev. **107**, 926 (2007).
[5] Jonathan Rivnay, Rodrigo Noriega, J. E. Northrup, R. J. Kline, M. F. Toney, and Alberto Salleo, Phys. Rev. B **83**, 121306(R) (2011).
[6] Jonathan D. Yuen, Reghu Menon, Nelson E. Coates, Ebinazar B. Namdas, Shinuk Cho, Scott T. Hannahs, Daniel Moses, and Alan J. Heeger, Nat. Mater. **8**, 572 (2009).
[7] M. Akai-Kasaya, Y. Okuaki, S. Nagano, T. Mitani, and Y. Kuwahara, Phys. Rev. Lett. **115**, 196801 (2015).
[8] Kamal. Asadi, Auke J. Kronemeijer, Tobias Cramer, L. Jan Anton Koster, Paul W. M. Blom, and Dago M. de Leeuw, Nat. Commun. **4**, 1710 (2013).
[9] L. Li, N. Lu, and M. Liu, J. Appl. Phys. **116**, 164504 (2014).
[10] A. J. Kronemeijer, E. H. Huisman, I. Katsouras, P. A. van Hal, T. C. T. Geuns, P. W. M. Blom, S. J. van der Molen, and D. M. de Leeuw, Phys. Rev. Lett. **105**, 156604 (2010).
[11] J. G. Park, Synth. Met. **135**, 299 (2003).
[12] Jiawei Wang, Jiebin Niu, Bin Shao, Guanhua Yang, Congyan Lu, Mengmeng Li, Zheng Zhou, Xichen Chuai, Jiezhi Chen, Nianduan Lu, Bing Huang, Yeliang Wang, Ling Li, and Ming Liu, Nat. Commun. **12**, 58 (2021).
[13] A. N. Aleshin, H. J. Lee, S. H. Jhang, H. S. Kim, K. Akagi, and Y. W. Park, Phys. Rev. B **72**, 153202 (2005).
[14] Hermann. Grabert and Ulrich. Weiss, Phys. Rev. Lett. **54**, 1605 (1985).
[15] R. Egger, Phys. Rev. Lett. **83**, 5547 (1999).
[16] Supplemental Material at http://link.aps.org/supplemental/10.1103/PhysRevLett.130.177001 for more details about devices processing techniques, electrical characterizations, simulations and modelings.
[17] Keehoon Kang, Shun Watanabe, Katharina Broch, Alessandro Sepe, Adam Brown, Iyad Nasrallah, Mark Nikolka, Zhuping Fei, Martin Heeney, Daisuke Matsumoto, Kazuhiro Marumoto, Hisaaki Tanaka, Shin-ichi Kuroda, and Henning Sirringhaus, Nat. Mater. **15**, 896 (2016).
[18] A. Alan Middleton and Ned S. Wingreen, Phys. Rev. Lett. **71**, 19 (1993).
[19] Klara Elteto, Eduard G. Antonyan, T. T. Nguyen, and Heinrich M. Jaeger, Phys. Rev. B **71**, 064206 (2005).
[20] Raghuveer Parthasarathy, Xiao-Min Lin, Klara Elteto, T. F. Rosenbaum, and Heinrich M. Jaeger, Phys. Rev. Lett. **92**, 076801 (2004).
[21] P. Sotta and D. Long, Eur. Phys. J. E **11**, 375 (2003).
[22] Yusi Xie, Dorota M. Artymowicz, Pietro P. Lopes, Ashlee Aiello, Duo Wang, James L. Hart, Elaf Anber, Mitra L. Taheri, Houlong Zhuang, Roger C. Newman, and Karl Sieradzki, Nat. Mater. **20**, 789 (2021).
[23] Adam M. Becker and Robert M. Ziff, Phys. Rev. E **80**, 041101 (2009).
[24] T. Potocar, S. Lorbek, D. Nabok, Q. Shen, L. Tumbek, G. Hlawacek, P. Puschnig, C. Ambrosch-Draxl, C. Teichert, and A. Winkler, Phys. Rev. B **83**, 075423 (2011).
[25] J. P. Clerc, G. Giraud, S. Alexander, and E. Guyon, Phys. Rev. B **22**, 2489 (1980).
[26] E. J. Garboczi, K. A. Snyder, J. F. Douglas, and M. F. Thorpe, Phys. Rev. E **52**, 819 (1995).